2024 IEEE International Conference on Robotics and Automation (ICRA 2024)
May 13-17, 2024. Yokohama, Japan

Rapid Resistography with Passive Overhead-perching Mechanism in an Unmanned Aerial System for Wood Structure Inspection

Shawndy Michael Lee[1†], Jingmin Liu[1†], Jer Luen Chien[1], Wei Hien Ng[1], Milven Lim[1], and Shaohui Foong[1], *Member, IEEE*

***Abstract*— This paper presents an aerial robotic platform for rapid remote elevated overhead-perching drill operations for wood health inspection. The platform features an innovative passive prismatic-gripper mechanism affixed to the aerial robot's top, facilitating overhead drilling. The primary aim is to enhance the safety and efficiency of elevated wood structure inspection using the resistography method, which involves drilling into wooden structures to identify internal voids. The research centers on two key enabling technologies: a gripper mechanism for secure attachment to target surfaces and a tethered drill configuration for drilling operations. The novel gripper mechanism enables drilling on large planar surfaces and even small beam-width structures. The paper concludes with discussions on design simulations and drill resistance experiments, highlighting the effectiveness of the proposed approach in detecting internal cavities within wooden structures.**

***Index Terms*— Resistography, Wood structure inspection, Tethered Aerial Robotics, Prismatic Gripper Mechanism, Internal cavity detection**

I. Supplementary Materials

Please see the following link for supplementary materials on the proposed system: https://youtu.be/GDH2jmWv_IA.

II. Introduction

In the pursuit of a collective effort to sustain the global forest, more trees are planted internationally, aiming to grow the forest area by 3%. Urban forests are increasingly recognized for their potential to yield psychological and societal advantages [1]. Nevertheless, with the proliferation of urban forest initiatives, there arises a critical need to safeguard the well-being of the flora, particularly in the context of mature and sizable trees. To address this concern, resistography emerges as a conventional yet non-destructive methodology employed for the assessment of internal structural conditions and the overall integrity of arboreal specimens, as well as timber and wooden constructions. The procedure entails the insertion of a slender needle or probe into the material of interest, with subsequent measurement of the encountered resistance [2]. In addition to the preservation efforts aimed at trees, numerous ancient heritage buildings in Asian nations, often constructed using timber as a primary material, are undergoing conservation endeavors. Within this context, resistography has found utility in the examination of the wooden components of these historic structures. Its role encompasses the identification and characterization of decay types and their specific locations within the timber elements. Although this method is non-destructive for the subject, ascertaining the condition of the structures often requires the resistograph to be manually used at an elevated height, putting the human user at risk of falls. Hence, safety measures such as scaffolds, harnesses, and/or mobile elevated work platforms (MEWPs) have to be set in place prior to operations. In recent years, the advancement of technologies has presented an array of opportunities for robotics to revolutionize traditional practices. Robotic solutions have the potential to tackle the stated problems: improving productivity, optimizing resource management, and minimizing workplace hazards. The field of aerial robotics, such as Unmanned Aerial Systems (UAS) specifically, has undergone significant advancements due to the increased accessibility, miniaturization, and affordability of electronics; transitioning from theoretical frameworks and research prototypes to commercially applicable products [3].

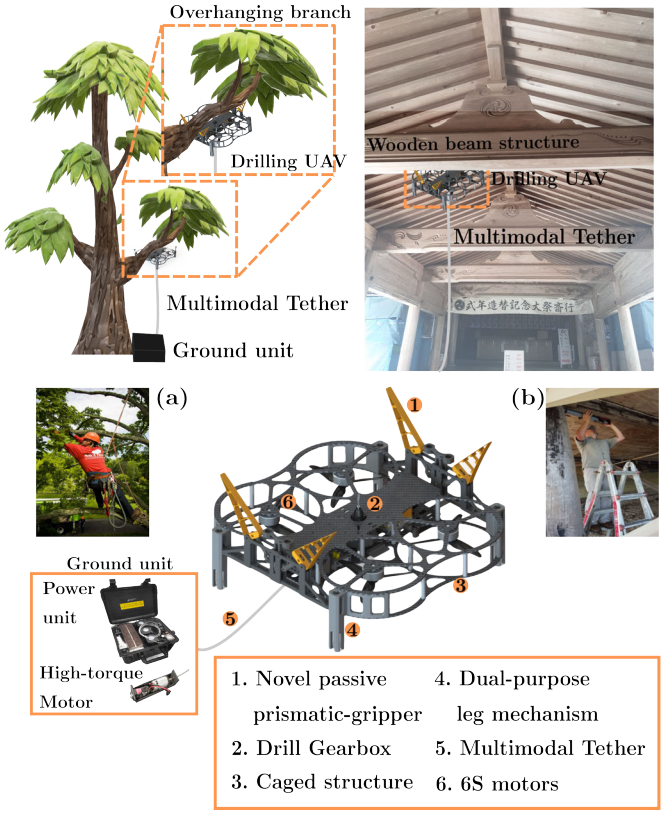

Fig. 1. Proposed robotic concept. Conventional resistography vs robotic concept: (a) Trees (thick overhanging branch). (b) Wooden structures.

[1]The authors are with the Department of Engineering Product Development, Singapore University of Technology and Design, Singapore Email: (foongshaohui,shawndy_lee)@sutd.edu.sg
† These authors contribute equally.

Modern UAS are able to carry out more sophisticated and complex tasks on behalf of humans, especially for jobs at elevated heights. Motivated by risk-free resistography, a novel variant of UAS for elevated remote drilling is presented in this paper, as illustrated in Figure 1.

III. Related Work

To check the health of the wooden structures at an elevation, there are two forms of wooden health inspection: non-invasive with visual inspection and minimal-invasive with resistography. There have been prior works on tree health diagnosis via visual inspection of tree cavities [4], [5], [6]. This form of tree health inspection is effective however it is heavily reliant on the presence of tree cavities which are uncommon and size-dependent. A more effective form is resistography which requires the task of micro-drilling into the wooden structure to check for the presence of internal cavities within the material, due to decay. To conduct resistography on high structures, the aerial robot must be able to perform two tasks: to perch itself onto the structure of interest and conduct the drilling operation.

A. Perching mechanisms

Firstly, Unmanned Aerial (UA) perching can be categorized into two distinct approaches namely, top-down (conventional) or bottom-up (overhead) approaches. The top-down approach, inspired by avians and insects, involves emulating their ability to land and rest on a perch after a flight, allowing for the UAS to maintain a low-to-no motor thrust [7], [8], [9]. The similarity between these works is that they employ a gripper-like end-effector or a metamorphic perching arm [10]. Conversely, the bottom-up approach involves the UAS perching itself onto the ceiling structure, akin to the perching behavior observed in bats, to exploit the ceiling effect to maintain optimal motor thrust in the perch state [11], [12], [13]. Hence, there is still a research gap in areas of the gripping mechanics of aerial robots that employ bottom-up approaches. The proposed perching mechanism takes inspiration from the bobbit worm's mandibles [14] that can be used for grasping onto overhead beam structures or branches for drilling while maintaining an optimal thrust proportional to the feed (or normal) force. The mechanism is designed to passively tighten its grasp with increased feed force, in this paper upward thrust delivered by the motors. This adaptation prevents counter-torque reaction due to the spinning of the drill bit; essentially improving the axial thrust forces. Therefore, it is essential to conduct a comprehensive analysis of the optimal drilling process in order to gain insights into which perching approach would be suitable for the task.

B. Drilling

Secondly, the UAS must be able to conduct remote drilling. During the drilling process, it is necessary to exert a feed force onto the rotating drill bit in order to penetrate into the material. Depending on the method of perching, the feed force that acts on the onboard drill can either be applied by its own body weight (for conventional perching) or by applied thrust [15] (for an overhead perching approach). While the feed force is directly proportional to the cutting force of the drill, a larger cutting force would require a higher torque motor. This usually leads to a larger drill hence, a larger UAS platform. For the proposed work, the overhead perching strategy is preferred due to the range of feed force that it can achieve. Thus, careful consideration must be given to the UAS's all-up weight (AUW) to reserve sufficient additional thrust to boost the feed force. [16] introduces a design methodology and workflow for constructing a UAS platform for its task.

To achieve this, the proposed design utilizes a multimodal tether system that incorporates a flexible shaft connected to an onboard drill bit. The drill bit is powered by a ground-based, high-torque motor. The flexible shaft allows for the effective transmission of torque along an irregular path. Flexible shafts have been extensively utilized in areas such as soft robotics manipulation [17] and surgical applications [18], [19]. Additionally, to maximize the efficiency of the UAS, a multimodal tether for power and drilling is adopted. Tethered UAS have been employed for a multitude of manipulation operations [20] namely, pressurised fluid ejection [21], [22], and aerial manipulation [23], [24], for their power efficiency and as safer alternatives to conventional, labor-focused methods.

C. Contributions

To our knowledge, this paper introduces a novel UAS capable of overhead perching, specifically designed for resistography applications. This paper will address the power transmission and feed force problem for elevated drilling scenarios with an overhead prismatic gripper that allows the robot to perch to the overhead beams or branches. Specifically, the contribution is presented as such:

- Design and development of the prismatic gripper end-effector mechanism for overhead perching and drilling on flat surfaces and beam structures.

This paper is organized as follows: in Section IV, the modelling for the overhead prismatic-gripper mechanism, and UAS optimized approach are developed. Simulation results are presented in Section V, and experimental results are reported in Section VI. Finally, Section VII concludes the paper.

IV. System Architecture

This section provides detailed insights into the mechanical versatility and capability of the prismatic-gripper mechanism, designed specifically to accommodate drilling on flat-surface ceilings and overhead beams. The novel passive overhead-perching UAS consists of the main aerial robot body, a multimodal tether system, and a prismatic-gripper mechanism for stabilization during overhead drilling.

A. Passive Prismatic-Gripper Design

The prismatic-gripper mechanism comprises 4 prismatic shafts mechanically coupled with 2 passive grippers where

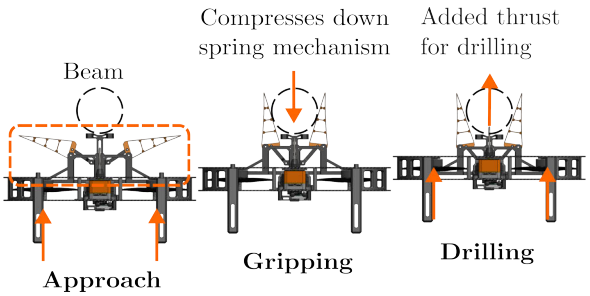

Fig. 2. Proposed Gripper Mechanism Process for Approach, Gripping and Drilling Phases.

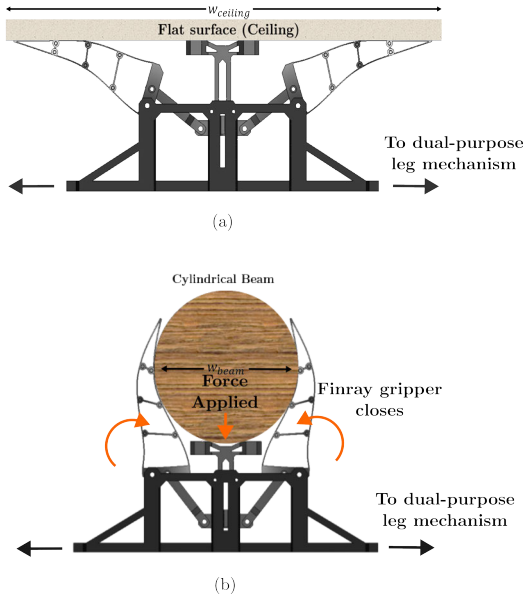

Fig. 3. Novel Passive Prismatic-Gripper. (a) Against (large and flat) ceiling surface. (b) Against (narrow) beam surfaces.

the shafts are loaded with individual springs as illustrated in Figure 3. Its purpose is to provide impact absorption, and stability when the UAS is in a perched state, as well as to enable the application of a range of drill feed forces. As such, it is imperative to optimize the drill feed force by studying the forces that act on the UAS. In the perched state, the UAS experiences the ceiling effect, where the proximity to the ceiling results in an increase in upward thrust. Exploiting this effect, the induced upward thrust acts as a beneficial additional feed force for the UAS. Consequently, the prismatic shafts also serve the purpose of acting as supplementary cushions, mitigating the impact on the UAS caused by the ceiling effect. As shown in Figure 4, the drill feed force is analogous to the forces that act in the positive z-axis direction z^+, is given by:

$$\mathbf{F}_{drill} = \sum \mathbf{F}_{z^+} = \begin{cases} \sum \mathbf{F}_t - \sum(\mathbf{F}_s + \mathbf{F}_{gs}) & \text{for beam} \\ \sum \mathbf{F}_t + \sum \mathbf{F}_{ce} - \sum \mathbf{F}_s & \text{for ceiling} \end{cases}, \tag{1}$$

where $\mathbf{F}_t$ is the thrust force, $\mathbf{F}_{ce}$ is the ceiling effect, $\mathbf{F}_s$ is the spring force, and $\mathbf{F}_{gs}$ is the gripper spring force. Since a beam is much smaller in dimensions as compared to a ceiling, the beam does not induce a significant ceiling effect.

1) Ceiling drilling: As the UAS approaches the ceiling, the ceiling effect will become prominent. This phenomenon is beneficial for the proposed UAS as any additional z+ force will aid in driving the total drill feed force, $\mathbf{F}_{drill}$. Adopted from [25], the ceiling effect force is given by:

$$\mathbf{F}_{ce} = \begin{bmatrix} F_{cex} \\ F_{cey} \\ F_{cez} \end{bmatrix} = \begin{bmatrix} 0 \\ 0 \\ 2\rho A \gamma^2 v_i^2 \end{bmatrix}, \tag{2}$$

such that,

$$F_{ce_z} = \sum_{i=1}^{4} 2\rho A \left(\frac{1}{2}(1-\alpha_1\delta^2) + \frac{1}{2}\sqrt{(1-\alpha_1\delta^2)^2 + \frac{\alpha_0}{\delta^2}} \right)^2 v_i^2, \tag{3}$$

where ρ is the air density, A is the cross-sectional area of the propeller disc (πr_{prop}^2) such that r_{prop} is the radius of the propellers, $\alpha_{0,1}$ are the dimensionless coefficients for non-axisymmetric flow and wake re-circulation respectively, v_i is the input velocity to the i-th motor, and δ is the propeller radius to ceiling ratio given by:

$$\delta = \frac{r_{prop}}{z_{ceiling}}, \tag{4}$$

For any additional thrust force acting on the UAS body in the perched state; zero change in spring compression length ($\Delta z_s = 0$):

$$\sum_{i=1}^{4} \mathbf{F}_{t_i} = k \begin{bmatrix} 0 \\ 0 \\ \sum \omega_i^2 \end{bmatrix} - \begin{bmatrix} 0 \\ 0 \\ mg \end{bmatrix}, \tag{5}$$

where i is the respective motor on the UAS, k is an appropriately-dimensioned constant, ω is the angular velocity of the motors and mg is the weight of the UAS.

The angular velocity can be obtained through the brushless motor electrical equation, given by:

$$\omega = \frac{V - I \cdot R}{K_e}, \tag{6}$$

where R is the electrical resistance of the motor's winding and K_e is the back EMF constant.

Once the prismatic shafts are loaded ($\Delta z_s > 0$), the spring force is active.

$$\sum \mathbf{F}_s = -\sum k_s \Delta z_s, \tag{7}$$

2) Beam drilling: The concept of beam drilling shares similarities with ceiling drilling, with the main difference being that the width of the target surface in beam drilling, w_{beam} is significantly narrower than the length of the passive gripper, $l_{gripper}$, also shown in Figure 3.

$$l_{gripper} \gg w_{beam}, \tag{8}$$

The top section of the prismatic-gripper mechanism comprises two fin-ray grippers. When the UAV perches against a beam, a downward force, $\mathbf{F}_{gs}$ is applied onto the gripper spring which activates and passively closes the fin-ray grippers hence, grasping onto the beam. This grasping action, due to the application of a load, is analogous to a loaded torsional spring where the spring rate is governed by:

$$k_{sr} = \frac{M}{\theta} = \frac{\mathbf{F}_{gs} \cdot l_{finray}}{\theta}, \tag{9}$$

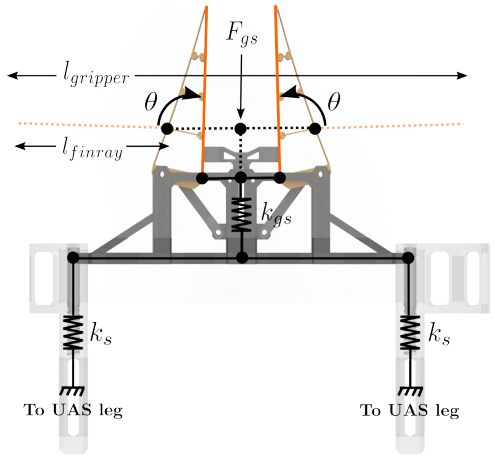

Fig. 4. Superimposed illustration of free body diagram and gripper mechanism where the bottom springs are connected to the UAS's legs.

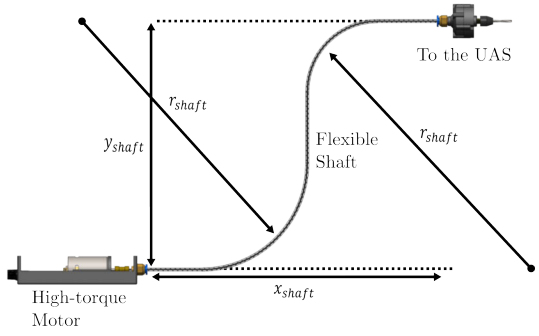

Fig. 5. Minimal Bending Radius of setup.

B. Mechanical Power Transmission

A pivotal enabling aspect of the presented concept is the utilization of a multimodal tether that facilitates the integration of a flexible drill shaft as illustrated in Figure 5. This obviates the need for the UAS to bear the weight of the onboard drill motor. Consequently, the drill motor can be positioned on the ground, thereby rendering the UAS drill motor agnostic. A proportional relationship exists between the operational torque and radius; as the radius decreases, the shaft's capability to withstand torque diminishes. Unlike conventional resistograph, in situations involving more pronounced bends, the internal wires experience heightened contact forces, leading to escalated levels of friction, heat generated, and mechanical strain. Nevertheless, to guarantee the optimal efficiency in the transmission of mechanical power, the minimal bending radius r_{shaft}, for such a drill shaft [26] is defined by:

$$r_{shaft} = \frac{x_{shaft}^2 + y_{shaft}^2}{4 \cdot y_{shaft}}, \tag{10}$$

where x_{shaft} represents the forward distance of the flexible shaft, from the drill motor, carried by the UAS; y_{shaft} is the vertical distance between the drill motor and UAS.

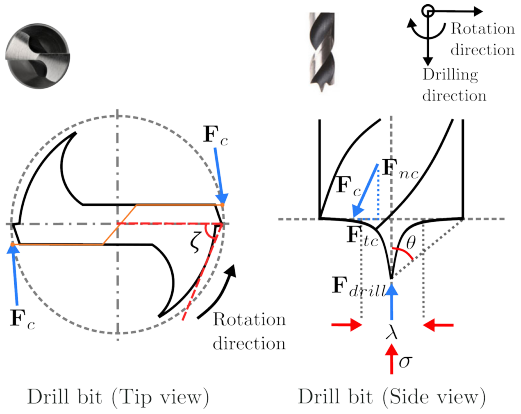

Fig. 6. Free Body Diagram of Drill Bit (Tip and Side views). $\mathbf{F}_c, \mathbf{F}_{nc}, \mathbf{F}_{tc}$ are the cutting force, normal cutting force, and tangential cutting force respectively. λ represents the length of the wear-flat, σ represents the localized compressive stress beneath the wear-flat.

C. Drill Resistance

The kinematic forces that act on the drill bit can be depicted by the free-body diagram (FBD) as illustrated in Figure 6. The conventional equation for drill resistance can be described by the summation of two components: one arising from material deformation and the other stemming from frictional interactions between the drill and the material:

$$R_{drill}(N) = R_{deformation} + R_{friction}, \tag{11}$$

To emulate a conventional resistograph, it is necessary to show that the drill resistance measurement (DRM) can be achieved. The DRM measures the force required to drill a hole at constant rotation (RPM) and lateral feed rate (mm/min). To validate the feed force for the drill gearbox, it is quintessential to quantify the amount of depth of cut per revolution d_c [27], [28], which is given by:
For a given input $\mathbf{F}_{drill}$,

$$d_c = f(\beta, \mathbf{F}_{drill}, RPM) = \frac{\beta}{RPM}, \tag{12}$$

where β is the feed rate, mm/min, and RPM is the revolution per minute of the drill bit. With Equation 12, the area of cut is:

$$A_c = w d_c, \tag{13}$$

where w is the width of the drill bit. The localized compressive stress beneath the wear-flat in the direction of drill σ is given by the maximum pressure p_{max}, over the ratio of the depth below the surface z, to contact radius a:

$$\sigma = \frac{-p_{max}}{\sqrt{(1 + \frac{z^2}{a^2})}}, \tag{14a}$$

$$p_{max} = \frac{3\mathbf{F}_{drill}}{2\pi a^2}, \tag{14b}$$

$$a = \sqrt[3]{\frac{3\mathbf{F}_{drill}}{8} \frac{(1-\nu_1^2)/E_1 + (1-\nu_2^2)/E_2)}{1/d_1 + 1/d_2}}, \tag{14c}$$

where E_1, ν_1, E_2, and ν_2 are the young's modulus and poisson's ratio for the high carbon steel drill bit and the wood

material respectively. The ratio of the normal and tangential components ζ is the back rake angle of the cutter shown in Figure 6, such that:

$$\zeta = tan(\theta), \tag{15}$$

Referencing Equations 11-15, for the case of drill bits commonly used in conservation (drill bits with just two cutters), the radius-independent drilling resistance $\frac{W}{r}$, is defined by:

$$R_{drill}(N) = \frac{\zeta \varepsilon \beta}{2RPM} + 2\sigma\lambda, \tag{16}$$

where the ε is the internal specific energy of the drilled material when considering the energy required to remove a certain volume of material during the drilling process.

V. Simulations

A. Fin Ray Gripper Optimal Design Analysis

The Fin Ray gripper, entirely 3D printed using PLA for flexibility and rigidity, maintains a minimal thickness (0.5mm for the shell, 0.8mm for cross beams). With dimensions W = 32.5mm, H = 10mm, and L = 103mm, it diverges from V-shaped designs, opting for a curved shell for better conformity to flat surfaces [29], [30]. Optimization involves three parameters: Arc Angle [$\angle$AOB = 5, 7.5, 10]°, Spacing [S= 11, 16.5, 22] mm between cross beams, and Incline Angle of cross beam [θ = -10, -5, 0, 5, 10]°, sequentially assessed via Solidworks Simulation. Figure 7 illustrates the gripper's maximum displacement during interactions with flat surfaces and gripping objects.

The optimization process begins by defining the arc angle, $\angle$AOB, in a gripper mechanism with stationary points A and B and a variable origin O. Observations show that an arc angle of $\leq$ 5° results in behavior similar to V-shaped grippers, incapable of conforming to flat surfaces. Prioritizing object gripping displacement, an arc angle of 7.5° is adopted. As spacing decreases, cross beams increase, reducing displacement; thus, a 22 mm spacing is chosen. Evaluating inclined angles from -10° to +10° reveals a trade-off: reduced gripper displacement while gripping versus exerting force on flat surfaces. Balancing design and performance, a median angle of 0° is adopted for optimal outcomes.

VI. Experiments

A. Mechanical Power Transmission Efficiency

To ensure that the tethered drill configuration is operating as efficiently as an onboard drill, a series of drill motor configurations for the flexible shaft were conducted on the RPM transmission: Straightened-unelevated (control), Coiled-unelevated, and Straightened-Elevated (ideal). The efficiency plot is illustrated in Figure 8. From this plot, the respective efficiency of the three configurations is compared to the input drill motor's RPM. For the ideal case, the Straightened-Elevated obtained about 95.72% efficiency as long as the bend-radius in Equation 10 is met while the Straightened and Coiled are at 98.49% and 83.41% respectively.

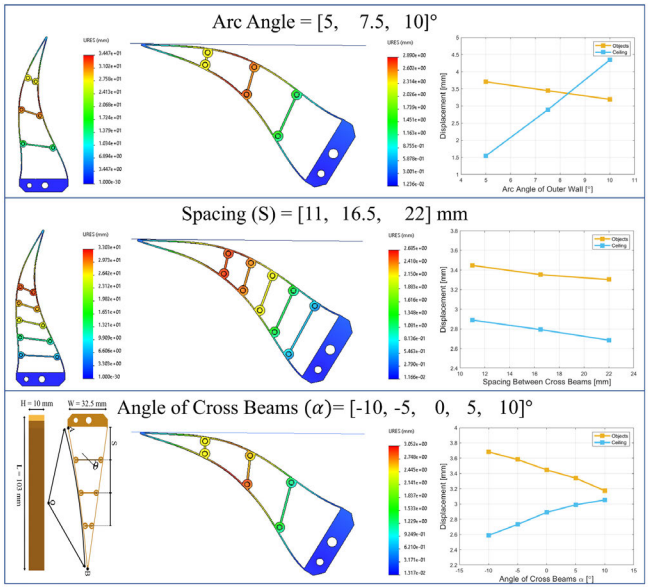

Fig. 7. Variance in Fin Ray Gripper Characteristics for Optimized Design.

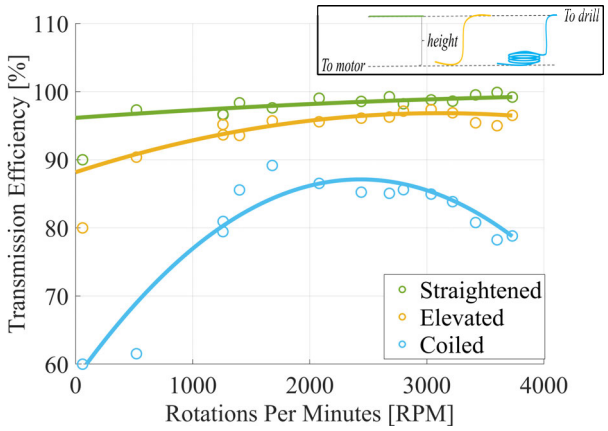

Fig. 8. Efficiency plot for Mechanical Power Transmission for the various tethered drill configurations.

B. Bench-top Experiments

Two bench-top experiments were conducted on the gripper mechanism as illustrated in Figure 9: a) Grasping on various diameter beams and b) Gripper force characterization were conducted to test the physical limitations of the mechanism. Figure 9a shows how the gripper conforms to the various diameters of the beam with ease and precision. Additionally, Figure 9b shows the relationship between the gripping force and the input feed force. These tests ascertain the usability of the gripper to provide added stability during the drilling process.

C. In-flight Drilling

Realistic mock-up drilling experiments of the respective beam and ceiling structures for real-world applications are conducted with the key experiment variables defined in Table I. The mock-up comprises a 10mm thick wooden structure for overhead-perch drilling. The aerial robot is flown

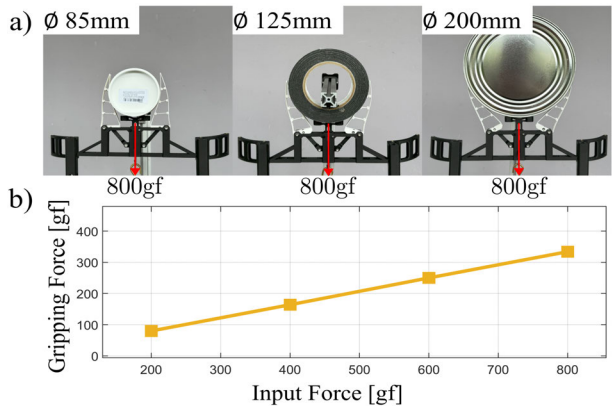

Fig. 9. a) Grasping on various diameter beams and b) Gripper force characterization were conducted to test the physical limitations of the mechanism.

TABLE I

TABLE OF DRILL RESISTANCE VARIABLES

Variable	Value
θ [rad], σ [Pa], ζ	0.698, 0.0025, 0.839
λ [mm], ε	0.002, 0.950
Thickness of the wood material [mm]	10
Variable	**[Lower bound, Upper bound]**
RPM	[2000, 3000]
$\mathbf{F}_{drill}$, [N]	[30, 50]
β [mm/min]	[0.470, 0.833]

manually to perch onto the target surface when the gripper mechanism conforms to the outline of the surface. Once it is perched, additional thrust is provided to allow the drill bit to cut into the material as shown in Figure 11. From Figure 10, the resistance drops once the drill bit penetrates across the material thickness, simulating the presence of a cavity within the material. The gripper mechanism also provides anti-torque capabilities and allows the UAS to concentrate the drill bit into the material of the beam.

VII. CONCLUSION AND FUTURE WORK

The proposed aerial robotic platform for remote elevated wood structure cavity inspection is presented, based on a caged-design quadcopter UAS equipped with a novel prismatic gripper mechanism for overhead drilling. The full goal of the project is to perch the UAS onto the target surface, align the drill bit to the surface, and detect possible cavities within a wooden structure through drilling resistance. Bench-top and preliminary experiments on realistic mock-up of wooden ceiling structures and beams have been realized and the results are promising however, more outdoor tests on actual trees and different composite wood materials are needed to validate the viability and feasibility of the wood health inspection. Future works will include control strategies for precise drilling.

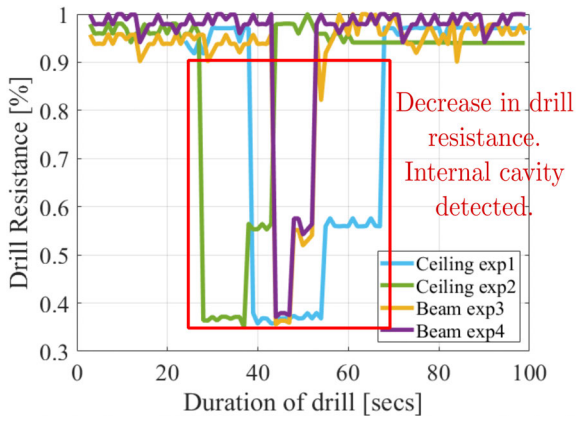

Fig. 10. Drilling Resistance [%] against the duration of drill [secs] on ceiling and beam surfaces during drill operation.

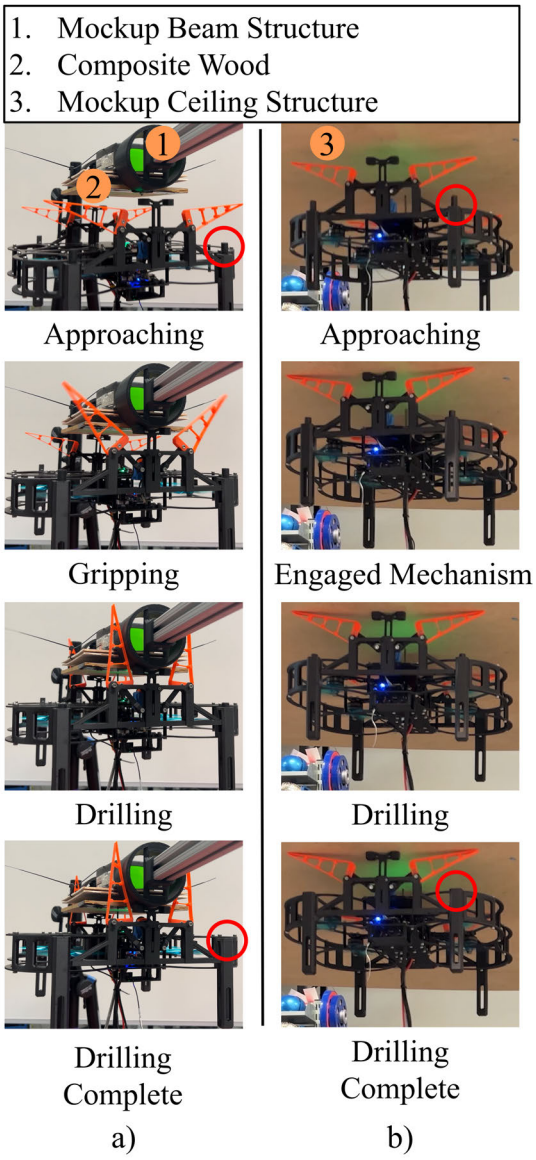

Fig. 11. Time-lapse series of drilling aerial robot in operation, proposed mechanism allows for stability and drilling. (a) Drilling process of wooden beam structure. Passive gripper mechanism holds onto to smaller-than-body structure, holds the UAS in position, and provides anti-torque capabilities. (b) Drilling process of wooden ceiling structure. Passive gripper mechanism conforms to the planar structure, increasing stability.

VIII. Acknowledgement

This research is supported by the Ministry of Education, Singapore, under its Academic Research Fund Tier 2 (MOE-T2EP50123-0004) and SUTD Kickstarter Initiative (SKI 2021_03_08).

References

[1] S. Kaplan. (2004). Some hidden benefits of the urban forest. In C.C. Konijnendijk, J. Schipperijn and K. H. Hoyer (Eds.) Forestry serving urbanised societies. (Selected Papers from conference jointly organized by IUFRO, EFI and the Danish Centre for Forest, Landscape and Planning in Copenhagen, 27-30 August 2002).Vienna, Austria: IUFRO (IUFRO World Series Vol. 14). Pp. 221-232.

[2] L. Orozco-Aguilar, C. R. Nitschke, S. J. Livesley, C. Brack, D. Johnstone, "Testing the accuracy of resistance drilling to assess tree growth rate and the relationship to past climatic conditions", "Urban Forestry Urban Greening", Vol 36, pp. 1-12, doi: 10.1016/j.ufug.2018.09.010.

[3] C. F. Liew, D. DeLatte, N. Takeishi, T. Yairi "Recent Developments in Aerial Robotics: A Survey and Prototypes Overview", Robotics, 2017, doi: 10.48550/arXiv.1711.10085

[4] K. Steich, M. Kamel, P. Beardsley, M. K. Obrist, R. Siegwart and T. Lachat, "Tree cavity inspection using aerial robots," 2016 IEEE/RSJ International Conference on Intelligent Robots and Systems (IROS), Daejeon, Korea (South), 2016, pp. 4856-4862, doi: 10.1109/IROS.2016.7759713.

[5] C. H. Tan et al., "Design and development of micro-aerial vehicle for tree inspections," 2017 IEEE International Conference on Cybernetics and Intelligent Systems (CIS) and IEEE Conference on Robotics, Automation and Mechatronics (RAM), Ningbo, China, 2017, pp. 593-598, doi: 10.1109/ICCIS.2017.8274844.

[6] J. Remm, A. Lõhmus, "Tree cavities in forests – The broad distribution pattern of a keystone structure for biodiversity", 2011, Forest Ecology and Management, 2011, Vol. 262, No. 4, pp. 579-585, doi: 10.1016/j.foreco.2011.04.028.

[7] S. Kirchgeorg and S. Mintchev, "HEDGEHOG: Drone Perching on Tree Branches With High-Friction Origami Spines," in IEEE Robotics and Automation Letters, vol. 7, no. 1, pp. 602-609, Jan. 2022, doi: 10.1109/LRA.2021.3130378.

[8] W. R. T. Roderick et al., "Bird-inspired dynamic grasping and perching in arboreal environments", Sci. Robot, vol. 6, no. 61, eabj7562(2021), doi:10.1126/scirobotics.abj7562, 2021.

[9] Paul H, Martinez RR, Ladig R, Shimonomura K. Lightweight Multipurpose Three-Arm Aerial Manipulator Systems for UAV Adaptive Leveling after Landing and Overhead Docking. Drones. 2022; 6(12):380. https://doi.org/10.3390/drones6120380

[10] Zheng, P., Xiao, F., Nguyen, P.H. et al. Metamorphic aerial robot capable of mid-air shape morphing for rapid perching. Sci Rep 13, 1297 (2023). https://doi.org/10.1038/s41598-022-26066-5, 2023.

[11] Kaiyu Hang et al., "Perching and resting—A paradigm for UAV maneuvering with modularized landing gears", Sci. Robot, vol. 4, pp. eaau6637(2019), doi:10.1126/scirobotics.aau6637, 2019.

[12] De Silva SC, Phlernjai M, Rianmora S, Ratsamee P. "Inverted Docking Station: A Conceptual Design for a Battery-Swapping Platform for Quadrotor UAVs", Drones, 2022; 6(3):56. https://doi.org/10.3390/drones6030056, 2022.

[13] J. Thomas, G. Loianno, K. Daniilidis, V. Kumar. (2015). "Visual Servoing of Quadrotors for Perching by Hanging From Cylindrical Objects", IEEE Robotics and Automation Letters (RAL), vol. 1. 1-1. doi:10.1109/LRA.2015.2506001, 2015.

[14] Y. Pan, Nara, Masakazu Löwemark, Ludvig Miguez-Salas, Olmo Gunnarson, Björn Iizuka, Yoshiyuki Chen, Tzu-Tung Dashtgard, Shahin. (2021). The 20-million-year old lair of an ambush-predatory worm preserved in northeast Taiwan. Scientific Reports. 11. 1174. 10.1038/s41598-020-79311-0.

[15] Drilling drone. (n.d.). Drilling Drone — ETH Zurich. https://ethz.ch/en/industry/industry/news/data/2022/10/drilling-drone.html

[16] Tan, C. H., Hölttä-Otto, K., and Foong, S. (July 25, 2022). "Efficient Design Guidelines for Innovative Aerial Robot Design." ASME. J. Mech. Des. November 2022; 144(11): 111403. https://doi.org/10.1115/1.4054938

[17] Q. Liu, X. Gu, N. Tan and H. Ren, "Soft Robotic Gripper Driven by Flexible Shafts for Simultaneous Grasping and In-Hand Cap Manipulation," in IEEE Transactions on Automation Science and Engineering, vol. 18, no. 3, pp. 1134-1143, July 2021, doi: 10.1109/TASE.2020.2997076.

[18] S. Treratanakulchai, E. Franco, A. Garriga-Casanovas, H. Minghao, P. Kassanos and F. R. y Baena, "Development of a 6 DOF Soft Robotic Manipulator with Integrated Sensing Skin," 2022 IEEE/RSJ International Conference on Intelligent Robots and Systems (IROS), Kyoto, Japan, 2022, pp. 6944-6951, doi: 10.1109/IROS47612.2022.9981437.

[19] M. Abayazid, M. Kemp and S. Misra, "3D flexible needle steering in soft-tissue phantoms using Fiber Bragg Grating sensors," 2013 IEEE International Conference on Robotics and Automation, Karlsruhe, Germany, 2013, pp. 5843-5849, doi: 10.1109/ICRA.2013.6631418.

[20] F. Ruggiero, V. Lippiello and A. Ollero, "Aerial Manipulation: A Literature Review," in IEEE Robotics and Automation Letters, vol. 3, no. 3, pp. 1957-1964, July 2018, doi: 10.1109/LRA.2018.2808541.

[21] Lee, S. M., Ng, W. H., Tang, E. Foong, S. (2022) Towards fluid force estimation of a water-jetting aerial robot with hybrid kinematics-force model. Journal of Field Robotics, 39, 805–826. https://doi.org/10.1002/rob.22079

[22] Lee SM, Ng WH, Liu J, Wong SK, Srigrarom S, Foong S. Flow-Induced Force Modeling and Active Compensation for a Fluid-Tethered Multirotor Aerial Craft during Pressurised Jetting. Drones. 2022; 6(4):88. https://doi.org/10.3390/drones6040088.

[23] R. Ladig, H. Paul, R. Miyazaki, and K. Shimonomura, "Aerial Manipulation Using Multirotor UAV: A Review from the Aspect of Operating Space and Force," J. Robot. Mechatron., Vol.33 No.2, pp. 196-204, 2021.

[24] J. L. Chien, L. T. L. Clarissa, J. Liu, J. Low and S. Foong, "Kinematic Model Predictive Control for a Novel Tethered Aerial Cable-Driven Continuum Robot," 2021 IEEE/ASME International Conference on Advanced Intelligent Mechatronics (AIM), Delft, Netherlands, 2021, pp. 1348-1354, doi: 10.1109/AIM46487.2021.9517606.

[25] C. Pakpong, H. Yi. 2019, "Ceiling Effects for Hybrid Aerial-Surface Locomotion of Small Rotorcraft", IEEE/ASME Transactions on Mechatronics, pp. 1-1. 10.1109/TMECH.2019.2929589, 2019.

[26] "Choosing READY-FLEX® Flexible Shafts Without Casing - With Couplings." S.S. White Technologies Inc. https://www.sswhite.net/ready-flex-without-casing (accessed Aug. 14, 2023).

[27] Dumitrescu, T.F., Pesce, G.L.A. Ball, R.J. Optimization of drilling resistance measurement (DRM) user-controlled variables. Mater Struct 50, 243 (2017). https://doi.org/10.1617/s11527-017-1113-8

[28] Dagrain, Fabrice Descamps, Thierry Poot, Benoit. (2010). Less-destructive testing of masonry materials: a comparison between scratching and drilling approaches.

[29] W. Xu, H. Zhang, H. Yuan and B. Liang, "A Compliant Adaptive Gripper and Its Intrinsic Force Sensing Method," in IEEE Transactions on Robotics, vol. 37, no. 5, pp. 1584-1603, Oct. 2021, doi: 10.1109/TRO.2021.3060971, 2021.

[30] Manoonpong, P., Rajabi, H., Larsen, J.C., Raoufi, S.S., Asawalertsak, N., Homchanthanakul, J., Tramsen, H.T., Darvizeh, A. and Gorb, S.N. (2022), Fin Ray Crossbeam Angles for Efficient Foot Design for Energy-Efficient Robot Locomotion. Adv. Intell. Syst., 4: 2270001. https://doi.org/10.1002/aisy.202270001, 2022.